Journal of Physics
Communications

PAPER • OPEN ACCESS

Implications of non-Markovian dynamics on information-driven engine

To cite this article: Obinna Abah and Mauro Paternostro 2020 *J. Phys. Commun.* **4** 085016

IOP Publishing J. Phys. Commun. 4 (2020) 085016 https://doi.org/10.1088/2399-6528/abaf99

Journal of Physics Communications

OPEN ACCESS

RECEIVED
25 July 2020

REVISED
8 August 2020

ACCEPTED FOR PUBLICATION
14 August 2020

PUBLISHED
25 August 2020

PAPER

Implications of non-Markovian dynamics on information-driven engine

Obinna Abah[1] and **Mauro Paternostro**

Centre for Theoretical Atomic, Molecular and Optical Physics, School of Mathematics and Physics, Queen's University Belfast, Belfast BT7 1NN, United Kingdom

[1] Author to whom any correspondence should be addressed.

E-mail: o.abah@qub.ac.uk and m.paternostro@qub.ac.uk

Keywords: non-Markovianity, quantum thermodynamics, collision model, information engine

Abstract

The understanding of memory effects arising from the interaction between system and environment is a key for engineering quantum thermodynamic devices beyond the standard Markovian limit. We study the performance of measurement-based thermal machine whose working medium dynamics is subject to backflow of information from the reservoir via collision based model. In this study, the non-Markovian effect is introduced by allowing for additional unitary interactions between the environments. We present two strategies of realizing non-Markovian dynamics and study their influence on the performance of the engine. Moreover, the role of system-environment memory effects on the engine work extraction and information gain through measurement can be beneficial in short time.

1. Introduction

The second law of thermodynamics is ubiquitous in nature: it stipulates that heat always flows from hot place to cold one. However, in 1867 Maxwell proposes the opposite with his idea of an intelligent demon to illustrate the statistical nature of the second law of thermodynamics [1]. The demon, with sufficient information about the microscopic motions of individual atoms and molecules, is able to separate the fast-moving ('hot') ones from the slow-moving ('cold') ones and induce the heat to flow from cold to hot, in apparent contradiction with the second law of thermodynamics. It took nearly a century to resolve this apparent paradox following a series of works, starting from Szilard's engine [2] through Landauer [3], Bennett [4] and others to clarify the link between the information recorded by the demon and the thermodynamic entropy, see [5]. The advances in nanotechnology have made the realization of Maxwell's thought experiment, Szilard's engine possible in recent time [6–8].

In addition to this, there has been a parallel line of development in the non-Markovian dynamic behavior of system interacting with reservoir. Theoretical advances have been made on the characterization of non-Markovian [9–11] as well as the verifications in various experimental setup [12–14]. The role of memory (non-Markovian) effects in understanding of information processing at both the classical and quantum level is currently attracting research interest [15–18]. Likewise, over the last few years , there has been an increase on the studies to understand or harness the non-Markovian effect on quantum thermodynamic machines [19–24]. Recently, studying the non-Markovian dynamic of a system has shed more light into the understanding of the Landauer principle [17].

Over the past few years, great effort has been devoted on studying the interplay between thermodynamics and quantum mechanics [25–30]. Remarkable progress has been made in understanding the non-equilibrium processes in thermodynamics as well as extending/generalizing the second law of thermodynamics to incorporates measurement and feedback driven processes [31–37]. Recently, the role of feedback control on information thermodynamic engine has been experimentally studied in different platform [38–43]. However, the understanding of the machine performance when the feedback engine protocol is performed by system exhibiting non-Markovian dynamics is still lacking. Although the self-consistent formulation of an interpretation of thermodynamic laws in the presence of measurements and feedback is still work in progress, and is attracting much attention, more practical issues such as the enhancement of the performance of cooling algorithms by feedback-based mechanisms are already under investigation and exploitation [44–47]. However, non-Markovian effects from the point of view of information flow have been examined [48] and a feedback-assisted work extraction demon has been proposed in [49].

In this paper, we investigate the implications of non-Markovian quantum dynamics on feedback-based information-driven machines described by collisional models (CM) [16, 50–55]. We discretize the continuous time evolution with a series of steps during which the system of interest couples/interacts with different components of a many-body quantum system that stimulates an extended environment. By properly controlling the intra-environment collisions/interactions one can pass from a purely Markovian dynamics to a strong non-Markovian regime. In fact, an extended control over the amount of non-Markovianity based on CM has been demonstrated experimentally in photonic setups [13, 56, 57]. Controllable non-Markovian quantum dynamics of an electronic spin qubit has been realized using a nitrogen-vacancy center in diamond [58–60]. In addition, the system under scrutiny is subjected to weak measurements implemented by weakly coupling it to an ancilla M that is then affected by strong projective measurements. This provides an elegant way to infer the state of effects on quantum system with only very little disturbance [61]. We show that memory can enhance the overall performance—work-done and information gain of the engine in a small number of discrete steps (i.e., short time). We remark that our framework/protocol can easily be implemented in a photonic experiment setup [13].

The rest of the paper is organized as follows. In section 2, we first present the measurement-based engine and then briefly discuss its thermodynamic analysis, section 2.2. In section 3 we introduce the CM-based model of non-Markovian dynamics and outline two different strategies for the tracking of the dynamics. Then, the characterization of the non-Markovian features is given in section 4.1, while the analysis of the feedback-driven engine in both Markovian and non-Markovian situation is reported in section 4.2. Finally, section 5 draws our conclusions.

2. Measurement-based thermo-machine

The system is initially brought into contact with a heat reservoir. It is then decoupled from the reservoir and and attached to a measuring apparatus. The latter consists of a quantum system, prepared in a given state, coupled to the system and subjected to projective measurements. The apparatus acquires information on the state of the system and depending on the result of the measurement performed on its state, a feedback operation is performed on the system. The setup consists of three components; system, reservoir and the ancilla.

2.1. Description of the protocol

We now introduce the protocol for the investigation of the effects that a process of information-gathering and feedback has on the capability of a system undergoing non-Markovian quantum dynamics to perform work, see figure 1. While *Step 1* and *2* of the scheme illustrated in figure 1 and described herein generate non-markovian dynamics, *Steps 3–6* illustrated below corresponds to the protocol in [35]. We proceed step by step, as follows:

Step 1: Initial preparation–System S and thermal reservoir(s) R are prepared in their respective equilibrium states at inverse temperature $\beta_i = 1/k_B T_i$, where $i = S, R$. The initial system-reservoir state is described by the density matrix

$$\rho_{SR} = \bigotimes_{i=R,S} \rho_i = \bigotimes_{i=R,S} \frac{e^{-\beta_i H_i}}{Z_i}, \tag{1}$$

where H_i denotes the Hamiltonian of element i and $Z_i = \mathrm{tr}[e^{-\beta_i H_i}]$ is the corresponding partition function. For simplicity, we consider the case in which the system and the reservoir are made of two-level systems.

Step 2: System-environment coupling–System and reservoir interact unitarily. In line with the usual formalism used in collisional models for quantum open-system dynamics [16, 37, 50–53, 62], in what follows we focus on a time-evolution operator of the partial-SWAP form such as

$$U_{SR} = e^{-i\tau}[\cos(2\tau)\mathbb{1}_4 + i\sin(2\tau)U_{sw}], \tag{2}$$

where τ is a dimensionless interaction time and U_{sw} is the two-particle SWAP transformation $|i, j\rangle_{SR} \xrightarrow{U_{sw}} |j, i\rangle_{SR}$ with $|i\rangle_S$ [$|j\rangle_R$] a state of the computational basis chosen for S [R]. This results in a sequential coherent exchange of information between the system and the element of the reservoir it has collided with for each collision/iteration. The S-R state after such unitary evolution is thus

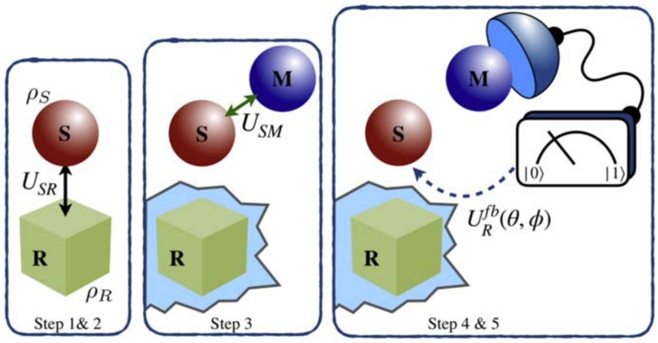

Figure 1. The various steps of the general protocol that we consider. The left panel illustrates the initial preparation and the unitary interaction between the system (S) and the reservoir (R). In the middle panel, the jagged light-blue area stands for the tracing-out of the environmental system. Then, in *Step* 3 the system interacts with the measuring apparatus . In the right panel, the information-gathering process in *Step* 4 consists of a projective measurement performed on the state of the ancilla M, which is projected onto the elements of its computational basis, such as $\{|0\rangle_M,\ |1\rangle_M\}$ in the case of a qubit. In *Step* 5, the feedback operation is performed.

$$\rho_{SR}^u = U_{SR}(\rho_S \otimes \rho_R)U_{SR}^\dagger. \tag{3}$$

In general, the joint dynamics embodied by U_{SR} gives rise to quantum correlations between system and environment. The environment is then discarded, leaving us with the reduced state of the system only

$$\rho_S^u = \mathrm{tr}_R[\rho_{SR}^u]. \tag{4}$$

Step 3: Pre-measurement–The system is then brought into contact with a measuring apparatus, i.e. an ancillary qubit M prepared in state ρ_M. The S-M coupling takes place according to the unitary transformation U_{SM}, which gives the joint density matrix

$$\rho_{SM}^{pm} = U_{SM}(\rho_S^u \otimes \rho_M)U_{SM}^\dagger, \tag{5}$$

where we call τ_m the dimensionless system-probe interaction time and H_{SM} the corresponding S-M coupling Hamiltonian such that $U_{SM} = e^{-i\tau_m(H_{SM}+H_S+H_M)}$. The coupling Hamiltonian can take different forms depending on the coupling direction. However, without loss of generality, we consider the case where we aim at performing projections onto the eigenstates of the Pauli spin matrix σ_z which can be achieved by preparing a probe qubit in the state $|0\rangle$ and then a controlled-NOT (CNOT) gate operation from the system to the probe before inferring the σ_z from the probe. Thus the unitary operator describing the general interactions between the system and probe is [63]

$$U_{SM} \equiv U_{\mathrm{CNOT}}(\tau_m) = \cos(\tau_m)\mathbb{1} \otimes \mathbb{1} - i\sin(\tau_m)\mathrm{CNOT}, \tag{6}$$

where CNOT $:= |0\rangle\langle 0| \otimes \mathbb{1} + |1\rangle\langle 1| \otimes \sigma_x$ is the definition of CNOT gate. For $\tau_m = 0$, there is no correlation between the system and probe whereas $\tau_m = \pi/2$ (CNOT up to the global phase $-i$) implies perfect correlation between the system and probe. The system and probe becomes partially correlated for $0 < \tau_m < \pi/2$.

Step 4: Measurement–This is the actual information-gathering step where the information on S acquired by the ancilla during *Step 3* is transferred to M via an actual measurement process. The latter is described by the complete set of projective operators $\{M_M^{(k)}\}$, defined in the Hilbert space of the ancilla M. Let us assume that the ancilla is initially prepared in one of its computational-basis states, i.e. $\rho_p^M = |p\rangle\langle p|_M$. The probability that outcome k is obtained as a result of such measurement is given by

$$P_k = \mathrm{tr}_{SM}[M_M^{(k)}\rho_{SM}^{pm}M_M^{(k)}] = \mathrm{tr}_S[\mathcal{F}_k\rho_S^u] \tag{7}$$

with $\mathcal{F}_k = \mathcal{E}_k^\dagger\mathcal{E}_k$ and $\mathcal{E}_k = {}_M\langle k|U_{SM}|p\rangle_M$ an element of the positive-operator value measure (POVM) induced on the system. The corresponding post-measurement state of the system reads

$$\rho_S^k = \mathcal{E}_k\rho_S^u\mathcal{E}_k^\dagger/P_k. \tag{8}$$

Concretely, we consider a *weak/gentle* projective measurement on the probe after the pre-measurement/interaction that gives only partial information about the system and thus only partially projects the system state. The projectors describing the local σ_z measurement on the probe are $M_M^0 := \mathbb{1} \otimes |0\rangle\langle 0|$ and $M_M^1 := \mathbb{1} \otimes |1\rangle\langle 1|$. However, for $\tau_m \ll 1$, the outcome $|0\rangle$ occurs with probability $P_0 \approx 1$, and the post-measurement state of the system is almost unchanged from the initial state [64], (cf appendix A). The resulting probability and post-measurement system state are

$$\rho_S^0 = \mathrm{tr}_M[M_M^0\rho_{SM}^{pm}M_M^0]/P_0, \quad P_0 = \mathrm{tr}_{SM}[M_M^0\rho_{SM}^{pm}M_M^0]. \tag{9}$$

In the context of photon polarization, one might direct single photons toward a weakly polarization dependent beam splitter to simulate such a measurement. In addition, it is possible to design a measurement protocol that only output post-selected state of a weak measurement on an NMR quantum information processor by controlled gate operation [65].

Step 5: Feedback control operation–Based on the outcome of the measurement at Step 4, the controller performs a conditional operation on the state of the system [31, 35]. The most general unitary transformation on a single-qubit state is a rotation $R_{\mathbf{n}}(\alpha) = \exp(-i\alpha\ \mathbf{n}\cdot(\sigma_x, \sigma_y, \sigma_z))$ that depends on an angle α about an arbitrary axis identified by the unit vector $\mathbf{n} = (\sin\theta\cos\phi,\ \sin\theta\sin\phi,\ \cos\theta)$, which has been written in polar coordinates specified by the polar angle θ and azimuthal one ϕ. By including a general global phase γ, such an arbitrary unitary rotation operator is $U_R^{fb}(\boldsymbol{\nu}) = \exp(i\gamma)R_{\mathbf{n}}(\alpha)$ and explicitly reads

$$U_R^{fb}(\boldsymbol{\nu}) = e^{i\gamma}\begin{pmatrix} \cos\frac{\alpha}{2} - i\cos\theta\sin\frac{\alpha}{2} & -i\sin\frac{\alpha}{2}\sin\theta e^{-i\phi} \\ -i\sin\frac{\alpha}{2}\sin\theta e^{i\phi} & \cos\frac{\alpha}{2} + i\cos\theta\sin\frac{\alpha}{2} \end{pmatrix} \tag{10}$$

with $\boldsymbol{\nu} := (\gamma,\ \alpha,\ \theta,\ \phi)$. In our case, the set of parameters upon which such rotation depends should be interpreted as conditioned on the outcome of the measurement performed, at Step 4, on the ancilla M. That is

$$\boldsymbol{\nu} \longrightarrow \boldsymbol{\nu}_k := (\gamma_k,\ \alpha_k,\ \theta_k,\ \phi_k). \tag{11}$$

The use of such conditioned rotation, which embodies our simple feedback control operation, delivers the state of the system

$$\rho_{S,k}^{fb} = U_R^{fb}(\boldsymbol{\nu}_k)\,\rho_S^k\, U_R^{fb^\dagger}(\boldsymbol{\nu}_k). \tag{12}$$

However, we remark that the feedback unitary operation could cancel the actual measurement effect depending on the choice of parameter $\boldsymbol{\nu}_k$, for more discussion, see appendix B.

Step 6: The reset–The system evolves independently and a fresh ancilla is made available to the next iteration of the protocol, which proceeds again from Step 1 onwards. This stage has no effect on the analysis that follows.

2.2. Thermodynamics of the machine

We proceed with the thermodynamic analysis of the protocol presented above, by calculating the changes in internal energy $E[\rho] \equiv \mathrm{tr}[H\rho]$ and entropy $S[\rho] \equiv -k_B\mathrm{tr}[\rho\ln\rho]$ of the system associated with the preparation, measurement and feedback-control steps.

First, after the system preparation (interaction with the reservoir), the change in the system internal energy is

$$\Delta E^u = E[\rho_S^u] - E[\rho_S] = \mathrm{tr}[H_S\,\rho_S^u] - \mathrm{tr}[H_S\,\rho_S], \tag{13}$$

and the change in system entropy reads

$$\Delta S^u = S[\rho_S^u] - S[\rho_S] = -k_B(\mathrm{tr}[\rho_S^u\ln\rho_S^u] - \mathrm{tr}[\rho_S\ln\rho_S]). \tag{14}$$

From the first law of thermodynamics, $\Delta E = W + Q$, and assuming that the heat exchange between the system and reservoir is governed by $Q_S^u = -Q_R^u$, which is reasonable in the absence of any channel for heat exchange other than the S-R interaction, the work done on/by the system can be written as $W^u = \Delta E^u + Q_R^u$, where $Q_R^u = \mathrm{tr}[H_R(\rho_R^u - \rho_R)]$ and $\rho_R^u = \mathrm{tr}_S[\rho_{SR}^u]$ is the marginal state of the reservoir after interaction.

For *Step 3*, the thermodynamic quantities are as follows. The variation of internal energy of the system reads

$$\Delta E^{pm} = E[\rho_S^{pm}] - E[\rho_S^u] = \mathrm{tr}[H_S\rho_S^{pm}] - \mathrm{tr}[H_S\rho_S^u], \tag{15}$$

where $\rho_S^{pm} = \mathrm{tr}_M[\rho_{SM}^{pm}]$ is the reduced state of the system after *Step 3*. The corresponding change in entropy of the state of the system is

$$\Delta S^{pm} = S[\rho_S^{pm}] - S[\rho_S^u]. \tag{16}$$

The work done during this process is $W^{pm} = \Delta E^{pm} + Q_m^{pm}$, where $Q_m^{pm} = \mathrm{tr}[H_M(\rho_M^{pm} - \rho_M)]$ and $\rho_M^{pm} = \mathrm{tr}_M[\rho_{SM}^{pm}]$ is the reduced state of the measuring apparatus with Hamiltonian H_M.

During the measurement stage, the information acquired from the system leads to entropy reduction. The resulting system state is out of equilibrium but its entropy and average energy are still well defined [32]. The gain of information about the system achieved through the measurement, after pre-measurement and measurement stage, is $I_g(\rho) = S(\rho_S^u) - P_k S(\rho_S^k)$ [35]. On the other hand, we have that the change in the internal energy during the measurement reads $\Delta E^m = E[\rho_S^k] - E[\rho_S^{pm}] \equiv W^m$.

Then, during the feedback step, the variation of system energy equals the work done by the system,

$$W^{fb} = \mathrm{tr}[H_S\rho_{S,k}^{fb}] - \mathrm{tr}[H_S\rho_S^k]. \tag{17}$$

Based on the thermodynamic energy conservation law during the preparation, measurement and feedback steps, we define the total work done on/by the system as

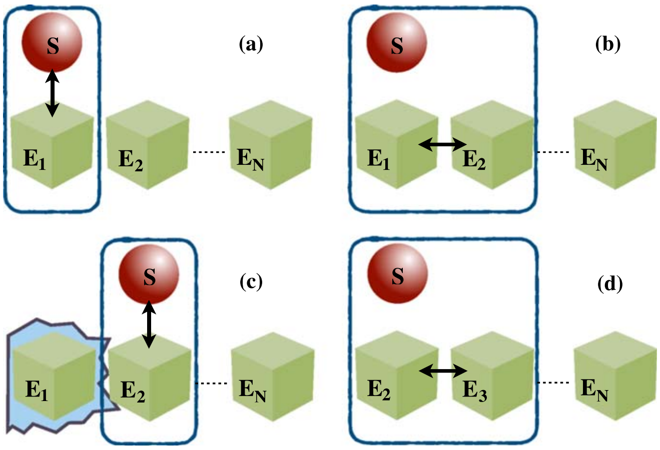

Figure 2. Schematic of non-Markovian dynamics via collision model for nearest sub-environment collisions. The system and the sub-environment particles are initially uncorrelated. In first step (a), system S interacts with E_1. In step, (b) E_1 interacts with E_2 thereby correlating the system and particles E_1 and E_2. Then in step (c), E_1 is traced away. After this the system interacts with E_2 before being isolated for the measurement and feedback processes (*Step 3–5*) entailed in *strategy-1*. Then, the system moves forward (d), while E_2 and E_3 interact.

$$\begin{aligned} W_t &= W^u + W^{pm} + W^m + W^{fb}, \\ &= W^u + \mathrm{tr}[H_S(\rho_{S,k}^{fb} - \rho_S^u)] + Q_m^{pm}. \end{aligned} \tag{18}$$

Equation (18) is beyond the second law of thermodynamics due to the correlation between the system and the memory. We remark that the form of such bound was first given in [31] for a discrete quantum feedback protocol (*Step 3-6*) starting and ending in equilibrium states, while details on the subject can be found in [37]. In section 3, we present the model that we use to account for non-Markovianity in the dynamics of S. Such effects can be characterized by work done on/by the system W^u. Then, we illustrate numerically the influence of the preparation on the information gain I_g and work extraction W_t in section 4.

3. Non-Markovian dynamics of the system—collisional based model

Here, we consider a situation where the system undergoes non-Markovian dynamics as a result of its interaction with the environment (taking place at steps 1 and 2 of our protocol). The realization of the dynamics that we decide to consider is that of collisional models, which offer great flexibility and richness of phenomenology [51, 52].

In particular, we consider the case in which the reservoir's memory mechanism arises from collisions between different elements of a structured, multi-party environment, following an interaction with the system. This scenario has been successfully used in the past to model memory-bearing mechanisms able to propagate to the environment information acquired on the state of the system [66]. More recently, this realization of memory-bearing effects has been used to assess the performance of a quantum Otto cycle having a harmonic system as a working medium [67]. Collisional models allow for the tracking of the dynamics of both system and environments, which in turn makes it possible to follow the ensuing emergence of the system-environment correlations responsible for memory effects [16, 50–55, 68]. They are thus invaluable methodological tools to assess the back-action of memory-bearing environments on the information-driven engine at the core of our study.

As anticipated above, we assume an environment R made out of a large number of elements, which we label $\{E_1, E_2,.., E_n\}$ and that we assume, for the sake of simplicity, to be identical. The total state of system and environment is initially factorized and the dynamics proceeds through as sequential collisions (interaction process) between S and an element E_n of the environment. These are followed by pairwise collisions/interactions between the elements of the-environment, as illustrated in figure 2. In [66], it has been shown that the degree of non-Markovianity of the reduced system dynamics depends on how the erasure of system-environment correlations is performed.

Here, we will consider two inequivalent schemes of tracing out the degree of freedom of the environment. The first scenario that we consider to compute the reduced dynamics of S requires the environmental particle E_n to be traced out when it has interacted with S and E_{n+1} but before the system interacts with E_{n+1}. In the second scenario, the reduced dynamics of the system is obtained by tracing out the environmental particle once it has interacted with system S. The remaining environmental particle interacts with the next homogeneous particle before the latter subsequently collides with the system. We also assume that the environment-environment interaction evolution is described by the unitary operator [16, 51–53]

$$U_{EE} = e^{-i\tau_e}[\cos(2\tau_e)\mathbb{1}_4 + i\sin(2\tau_e)U_{sw}], \tag{19}$$

which describes another partial-SWAP gate between two consecutive elements of the environment, parameterized by the dimensionless interaction time τ_e.

The first scenario (which we term *strategy-1*) that we consider involves tracing out particle E_n after it has collided with E_{n+1}, as exemplified in figures 2(a)–(c). It starts with a collision between S and E_n, modelled through the unitary operation U_{SR} in equation (2), which delivers the joint state

$$\rho_{SE_n} = U_{SR}(\rho_S \otimes \rho_{E_n})U_{SR}^{\dagger}. \tag{20}$$

The three particles S, E_n and E_{n+1} then become correlated through the intra-environment interaction $U_{E_nE_{n+1}}$ in equation (19), after which particle E_n is traced out. This results in the bipartite S-E_{n+1} state

$$\rho_{SE_{n+1}} = \mathrm{tr}_{E_n}[U_{EE}(\rho_{SE_n} \otimes \rho_{E_{n+1}})U_{EE}^{\dagger}]. \tag{21}$$

The marginal state of the system is computed after the interaction with E_{n+1}. Thus, *strategy-1* prepare the system in state

$$\rho_S^u = \mathrm{tr}_{E_{n+1}}[U_{SR}\,\rho_{SE_{n+1}}U_{SR}^{\dagger}]. \tag{22}$$

We remark that retaining the correlations up to the third environment—which corresponds to the systematic collision with the environmental components E_n, E_{n+1}, and E_{n+2} as in figure 2—does not change the resulting dynamics [54]. At the end of the system-environment interaction, the engine-protocol steps [step 3–6] are performed before the system collides with another fresh environment.

In the second scenario, dubbed *strategy-2*, the correlation established between S and E_n is removed before the intra-environment interaction $E_n - E_{n+1}$. The states achieved at each stage of *strategy-2* are thus as follows. First, the collision between system and E_n occurs, which gives the state

$$\rho_{SE_n} = U_{SR}(\rho_S \otimes \rho_{E_n})U_{SR}^{\dagger}, \tag{23}$$

and their resulting marginals $\rho_{S'} = \mathrm{tr}_{E_n}[\rho_{SE_n}]$ and $\rho_{E_n'} = \mathrm{tr}_S[\rho_{SE_n}]$ for the system and E_n respectively. Then, the marginal state of the E_{n+1} sub-environment component after the intra-environment collision is

$$\rho_{E_{n+1}'} = \mathrm{tr}_{E_n'}[U_{EE}(\rho_{E_n'} \otimes \rho_{E_{n+1}})U_{EE}^{\dagger}]. \tag{24}$$

The resulting state of the system prepared by *strategy-2* becomes

$$\rho_S^u = \mathrm{tr}_{E_{n+1}'}[U_{SR}\,(\rho_{S'} \otimes \rho_{E_{n+1}'})U_{SR}^{\dagger}]. \tag{25}$$

This scenario clearly differs from the first one in both the number of particles being involved, and the amount of correlations that are retained as a result of the system-environment interaction. In turn, this influences the non-Markovian features of the dynamical maps applied to S and arising from the implementation of such strategies.

To quantify the degree of non-Markovianity of the reduced system dynamics undergone by S, we employ the measure for non-Markovianity proposed in [9] which is associated with back-flow of information from the environment to the system. This is based on the time behavior of the trace distance between two different initial quantum states of S, that is

$$D(\rho_1, \rho_2) = \frac{1}{2}||\rho_1 - \rho_2||, \tag{26}$$

where $||\rho|| = \mathrm{tr}[\sqrt{\rho^{\dagger}\rho}]$ is the trace norm of operator ρ and $\rho_{1,2}$ are two density matrices of S. For Markovian dynamics, $D(\rho_1, \rho_2)$ monotonically decreases with time for any pair of initial states $\rho_{1,2}(0)$. On the contrary, a dynamical process is signalled as non-Markovian if there is a pair of such states for which this quantity exhibits a non-monotonic behaviour.

4. Analysis of non-Markovianity and its role in the performance of the engine

Now we present the numerical analysis of the non-Markovian dynamics of the collision model for both strategies described above and then, their role on the thermodynamics of the engine. In the remainder of the paper, we will assume both the system and reservoir to be two-level systems with Hamiltonian $H_i = \omega_i\sigma_i^{(j)}/2$, with the thermal state density matrix of the form $\rho_i(\sigma_i^{(j)}) = \exp(-\beta_i H_i)/Z_i$, where $j = x, y, z$ is a label for the j-Pauli spin operator of particle $i = S, R$, and β_i is the corresponding inverse temperature. We remark that, provided that the frequencies are positive ($\omega_R > \omega_S$) and the inverse temperatures are the same, the results presented hold qualitatively.

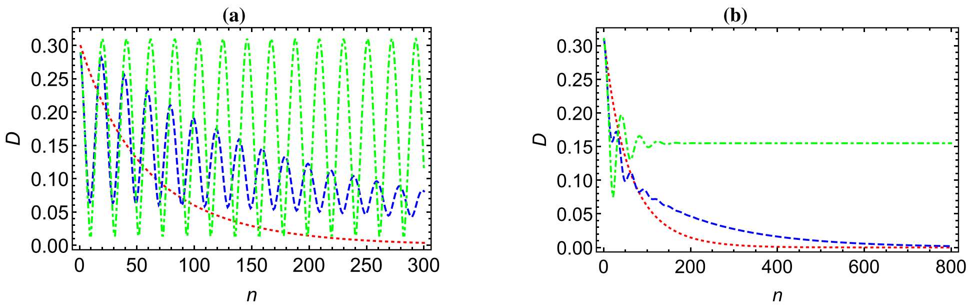

Figure 3. The trace distance D between evolved system states as a function of the number of collision iteration n with the environment for both strategies. Left (a) [right (b)] panel are the results for the *strategy-1* [*strategy-2*]. We have considered the initial states $\rho_{S1}(\sigma_S^z)$ and $\rho_{S2}(\sigma_S^y)$, while the sub-environments are prepared in $\rho_R(\sigma_R^z)$. The red dotted curve corresponds to the Markovian situation, $\tau_e = 0.0$, while the blue dashed and green dot-dashed curves represent the non-Markovian dynamics with the dimensionless inter-environmental coupling time $\tau_e = 10\pi/43$ and $\tau_e = \pi/4$ respectively. The system-environment interaction time is $\tau = \pi/42$ for weak coupling and the system and environment frequency parameters are $\omega_S = 1$ and $\omega_R = 3$, while their inverse temperature is fixed at $\beta_S = \beta_R = 0.94$.

4.1. Non-Markovianity features from both strategies

We numerically analyze the behaviour of the trace distance $D(\rho_{S_1}, \rho_{S_2})$ as the collision-based model for system-environment interactions are repeatedly executed. This analysis will elucidate how to arrange the dynamics to be a non-Markovain using different strategies described in section 3 and corresponds to the first two steps of the engine protocol, see section 2.1. We present the behaviour of the trace distance in equation (26) for two initial states prepared at $\rho_{S1}(\sigma_S^z)$ and $\rho_{S2}(\sigma_S^y)$. We have assumed that all environmental particles/qubits are initialized in the state $\rho_R(\sigma_R^z)$. The large value of the trace distance corresponds to distinguishable states while a null value is achieved when the states are identical.

Figures 3(a) and (b) show the differences between the two strategies addressed in this study. For purely Markovian dynamics ($\tau_e = 0$, red dotted curves), the trace distance decreases monotonously while switching on the inter-environment interaction times ($\tau_e \neq 0$, blue dashed and green dot-dashed curves) results in revivals that are evidence of non-Markovianity. In fact, this system-environment interaction produces a backflow mechanism—which is seen as oscillations of the trace distance that fades out in the large number of collisions with fresh ancilla. We observe that the strong environment-environment interaction time $\tau_e = \pi/4$ corresponds to a full state-swap between two consecutive environment particles that results in a non vanishing trace distance, see the green dot-dashed curves in figures 3(a) and (b). It can be seen that the oscillations are more persistent in *strategy-1* (figure 3(a)) but fade out to a non-zero value in the *strategy-2*, see figure 3(b). While the non-Markovian dynamics persists for both strategies in strong intra-environment interaction, the intermediate coupling strength shows a clear dependence of the non-Markovian nature on the way information/correlation is developed via collisions. For a weaker environment-environment particle interaction times $\tau_e < \pi/4$, both strategies trace distance decreases as the number of environmental collision increases, see blue dashed curves in figure 3. For more extensive discussion on the way information is exchanged between the system and environment for the two strategies and their differences/superiority, see [54, 66].

4.2. Feedback-driven engine analysis

Let us now evaluate the influence of non-Markovianity on the performance of the measurement-based machine described in section 2 above. We consider a two-level system initially prepared in the state $\rho_S(\sigma_S^z)$ and many identical subenvironment prepared in the state $\rho_R(\sigma_R^z)$. The measurement ancilla is prepared in the state $\rho_0^M = |0\rangle\langle 0|$ with the system-measurement apparatus unitary evolution U_{SM} characterized by the coupling of the form in equation (6). Then, a feedback rotation operation of the form $U_R^{fb}(\pi/2, \pi/4, \pi/4, \pi/4)$ is performed on the system state after the measurement outcome. The thermodynamic quantities, such as work extraction and quantum information gain are numerically calculated and presented in figure 4. The quantum information gain gives a measure of the correlations between the system and the measurement apparatus while the work extraction deals with the energy exchange during the preparation, measurement and feedback operation. Note that a deeper and more complete theoretical explanation of the link between the thermodynamic quantities is still missing.

In figure 4, the feedback engine performance, work performed by the engine protocol and the corresponding quantum mutual information associated with the measurement step, as a function of repeated collision are presented for the two different non-Markovian strategies described above. For the Markovian dynamics ($\tau_e = 0$, red dotted curves in figures 4(a) and (b)), the total work done and quantum mutual information increases as the system-environment interactions times grow until it they reach constant values many collision

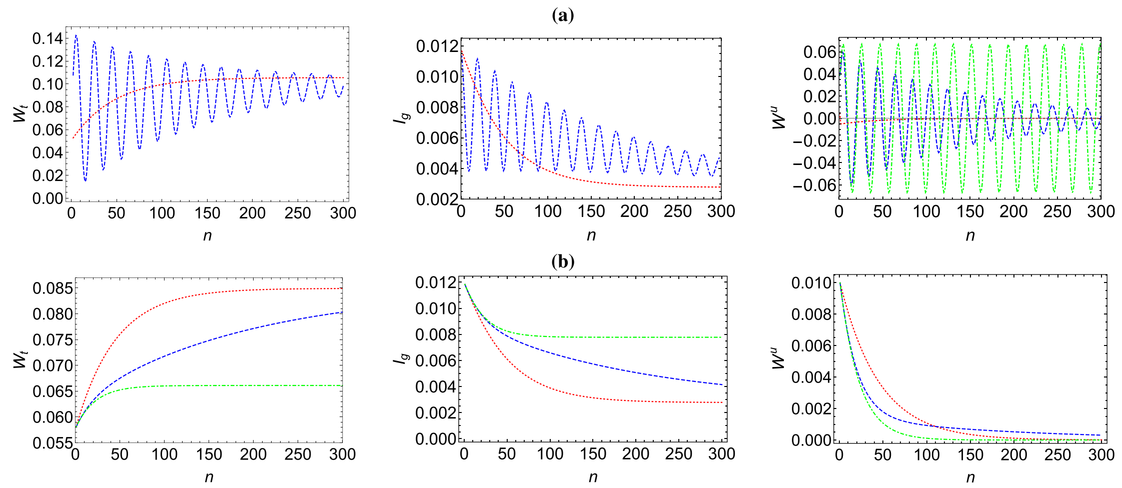

Figure 4. Feedback driven engine performance: The total work done W_t, the quantum information gain I_g and the work done during preparation step W^u as a function of number of collision n with the environment. The upper panel (**a**) corresponds to *strategy-1* while the lower panel (b) is for *strategy-2*. The red dotted curve corresponds to the Markovian dynamics, $\tau_e = 0.0$ while the blue dashed curve represent the non-Markovian dynamics, $\tau_e = 10\pi/43$. The green dot-dashed curve represent the full swap non-Markovian dynamics, $\tau_e = \pi/4$. The system-environment interaction time is $\tau = \pi/42$ for weak coupling and the system and environment frequencies parameters are $\omega_S = 1$ and $\omega_R = 3.0$ respectively. The system-probe interaction time is $\tau_m = \pi/14$ and $\beta_S = \beta_R = 0.94$. In addition, the heat associated with the pre-measurement step is $Q_M^{pm} \approx \pm 4 \times 10^{-16}$ for the chosen parameters.

iteration. For the *strategy-1*, figure 4(a), as the system dynamics is prepared to be non-Markovian, an oscillatory behaviour which vanishes in the long collision time are observed for both engine performance quantities—work done and information gain. The non-Markovian feature is strong at short collision times and can exceed their Markovian counterpart. However, the intermediate system-environment iteration is marked with suppression of the engine performance due to memory effect. For the non-swap environment-environment interactions (e.g $\tau_e = 10\pi/43$), the total work done and information gain approach the Markovian values after many number of collisions, see figure 4(a). This results from the reduction of information back-flow and the saturation point corresponds to the collision iteration number that the thermodynamic quantities (ΔE^u, Q^u and W^u) during the preparation step vanishes. In addition, we remark that including the work done on/by the system during the preparation (*Step-1 & 2*) does not affect our results qualitatively. Moreover, the system work done during the preparation W^u exhibit similar oscillatory behaviour but alternates between positive and negative values, see right panel of figure 4(a).

Figure 4(b) shows the work-extraction and information gain through measurement resulting from implementation of *strategy-2*. We observe that such non-Markovian dynamics scenario ($\tau_e \neq 0$) gives rise to non oscillatory behaviour contrary to *strategy-1* and the amount of work extraction and information gain quantities never exceed the Markovian one. This behaviour is akin to the observation in the trace distance figure 3(b), in which the *strategy-2* oscillation are short time leave. Interestingly, for strong environment-environment interaction time $\tau_e = \pi/4$, the total work done and information gain saturate to finite value that is lower than the Markovian case, see the green curves in figure 4(b). Likewise, the saturation occurs at a vanishing change in the system work done, $\Delta W^u = 0$. For more iterations with fresh environments under weaker interaction environment-environment time $\tau_e = 10\pi/43$, the quantities attain the Markovian values. However, it takes different amount of environment collisions to achieve the Markovian conditions for both strategies.

Strategy-1 is evidently superior to *strategy-2* in setting a nonzero degree of non-Markovianity as well as oscillatory behaviour of the engine performance (work done and information gain). The oscillations may lead to enhanced work and information gain compared to the Markovian dynamics ($\tau_e = 0$). Interestingly, even the small oscillatory behaviour observed for the strong system-environment interaction time based on *strategy-2* (see, trace distance of figure 3(b)) did not leave a trace in the performance analysis. However, the resulting work after system-environment interaction W^u has a behaviour that is reminiscent of the quantum information gain of the engine protocol. We remark that the differences depend on the way system-environment correlations are accounted for at the system preparation stage (i.e, *Step 1 & 2*).

5. Conclusion

We have investigated the interplay between memory effects and performance of a feedback-driven quantum engine. The engine setup consists of system, reservoir and measurement probe which we have modelled as set of

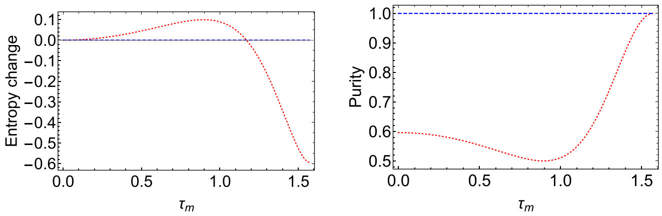

Figure A1. The change in entropy and purity as a function of interaction time τ_m after a projective measurement performed on the state of the ancilla M, which is projected onto the $\{|0\rangle_M\}$ of its computational basis. The red-dotted [blue-dashed] curves corresponds to the system [probe] change in entropy (left panel) and the purity (right panel) respectively.

two-level systems. We have employed the trace distance as a measure of memory effects (non-Markovianity) to illustrate two strategies of realizing non-Markovian dynamics. We have observed that memory effects can enhance the performance—*work* and *information gain*—of feedback-driven engine for a small number of system-environment collisions. However, the performance decreases as the number of collisions grows and approaches the Markovian value for a very large number of collisions. Besides shedding light on the interplay between non-Markovianity and measurement driven engine, this study suggest more theoretical effort to understand the role of memory on information thermodynamics. Furthermore, it will be interesting to understand the influence of non-Markovian dynamics that arise from the intrinsic uncertainties associated with measurement e.g. quantum projection noise [69].

Acknowledgments

We thank Steve Campbell for his helpful comment on the manuscript. The authors acknowledge the support by the Royal Society (Grant Numbers NF160966 and NI160057), the Royal Commission for the Exhibition of 1851, the SFI-DfE Investigator Programme grant (Grant 15/IA/2864), and the H2020 Collaborative Project TEQ (Grant Agreement 766 900).

Appendix A. Weak measurement

Here, we present the weak measurement of a two-level system described by the Hamiltonian $H_S = \omega_S \sigma_S^z/2$ is prepared in thermal state $\rho_S = \exp(-\beta_S H_S)/\mathrm{tr}[\exp(-\beta_S H_S)]$. We consider a probe qubit in the $|0\rangle$ state, measuring the system in its computational basis after unitary evolution $U_{SM} = \cos(\tau_m)\mathbb{1} \otimes \mathbb{1} - i\sin(\tau_m)\mathrm{CNOT}$ for interval $0 < \tau_m < \pi/2$. The post-measurement state of the system is;

$$\rho_S^0 = \mathrm{tr}_{\mathrm{M}}[M_M^0 \rho_{SM}^{pm} M_M^0]/P_0, \quad P_0 = \mathrm{tr}_{\mathrm{SM}}[M_M^0 \rho_{SM}^{pm} M_M^0]. \tag{A1}$$

where M_M^0 is the measurement projector. Assuming a system with inverse temperature $\beta = 0.98$ and frequency $\omega_S = 1.0$, we have the initial entropy $S_S = -k_B \mathrm{tr}[\rho_S \ln \rho_S] \approx 0.593$ and purity $P_S \approx 0.596$. Needless to say, the entropy and purity of the probe in a pure state are zero and one respectively. Then, the resulting changing in entropy and purity of the system as well as the probe after the weak measurement as a function of interaction time are shown in figure A1. We see that the system entropy and purity are influenced by the interaction time whereas the corresponding probe's quantities remain unchanged.

Appendix B. Feedback protocol

This involves the unitary rotation of resulting measurement outcome as described in section 2.1. Here illustrate that depending on the choice of feedback operation or rotation matrix, the work extracted by the process can be increased/decreased. For the case considered in A, the internal energy of the quantum system after measurement is $E_{ini} \approx -0.21$ for $\tau_m = 0.25$. In figure B1, we present the internal energy variation $E[\rho_{fb}] = \mathrm{tr}[H_s \rho_{fb}]$ as function angle of rotations after a unitary operation $U_R^{fb}(\gamma, \alpha, \theta, \phi)$ characterized by equation (10) and the system final state $\rho_{fb} = U_R^{fb} \rho_{ini} U_R^{fb^\dagger}$. From left panel of figure B1, we see that the maximum positive energy corresponds to the rotation matrix $U_R^{fb}(\pi/2, \pi, \pi/2, 0 - \pi/2)$. We note, when $\alpha = \pi/2$, the maximum value of the energy is zero. On the other hand, when the angles (θ, α) are varied, the energy varies from $E[\rho_{fb}] \approx -0.2$ to 0.2. Therefore, some choice of angles can result in no contribution of the feedback operation to the total work done, i.e $W_{fb} = E[\rho_{ini}] - E[\rho_{fb}]$.

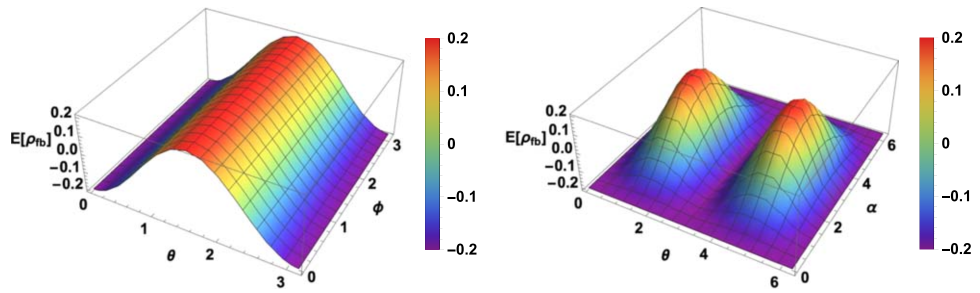

Figure B1. The final energy of the system as a function of rotation angles following a unitary feedback operation. The left panel shows the energy as function of the angles variation (θ, ϕ) for $\gamma = \pi/2$ and $\alpha = \pi$ while the right panel represent variation of the angles (θ, α) for $\gamma = \pi/2$ and $\phi = \pi/2$. For both plots, the measurement interaction time parameter $\tau_m = 0.25$.

ORCID iDs

Obinna Abah https://orcid.org/0000-0003-0193-4860
Mauro Paternostro https://orcid.org/0000-0001-8870-9134

References

[1] Leff H S and Rex A F 2002 *Maxwell's Demon 2 Entropy, Classical and Quantum Information, Computing* (UK: CRC Press, Taylor & Francis Group) ist ed.
[2] Szilard L 1929 *Zeitschrift für Physik* **53** 840
[3] Landauer R 1961 *IBM J. Res. Dev.* **5** 183
[4] Bennett C H 1982 *Int. J. Theor. Phys.* **21** 905
[5] Parrondo J M R, Horowitz J M and Sagawa T 2015 *Nat. Phys.* **11** 131
[6] Toyabe S, Sagawa T, Ueda M, Muneyuki E and Sano M 2010 *Nat. Phys.* **6** 988
[7] Bérut A, Arakelyan A, Petrosyan A, Ciliberto S, Dillenschneider R and Lutz E 2012 *Nature* **483** 187
[8] Koski J V, Maisi V F, Sagawa T and Pekola J P 2014 *Phys. Rev. Lett.* **113** 030601
[9] Breuer H-P, Laine E-M and Piilo J 2009 *Phys. Rev. Lett.* **103** 210401
[10] Rivas A, Huelga S F and Plenio M B 2010 *Phys. Rev. Lett.* **105** 050403
[11] Lorenzo S, Plastina F and Paternostro M 2013 *Phys. Rev.* A **88** 020102
[12] Liu B-H, Li L, Huang Y-F, Li C-F, Guo G-C, Laine E-M, Breuer H-P and Piilo J 2011 *Nat. Phys.* **7** 931
[13] Chiuri A, Greganti C, Mazzola L, Paternostro M and Mataloni P 2012 *Sci. Rep.* **2** 968
[14] Souza A, Li J, Soares-Pinto D, Sarthour R, Oliveira S, Huelga S, Paternostro M and Semião F 2013 arXiv:1308.5761
[15] Reeb D and Wolf M M 2014 *New J. Phys.* **16** 103011
[16] Lorenzo S, McCloskey R, Ciccarello F, Paternostro M and Palma G M 2015 *Phys. Rev. Lett.* **115** 120403
[17] Pezzutto M, Paternostro M and Omar Y 2016 *New J. Phys.* **18** 123018
[18] Hamedani Raja S, Borrelli M, Schmidt R, Pekola J P and Maniscalco S 2018 *Phys. Rev.* A **97** 032133
[19] Gelbwaser-Klimovsky D, Erez N, Alicki R and Kurizki G 2013 *Phys. Rev.* A **88** 022112
[20] Mukherjee V, Giovannetti V, Fazio R, Huelga S F, Calarco T and Montangero S 2015 *New J. Phys.* **17** 063031
[21] Chen H-B, Chiu P-Y and Chen Y-N 2016 *Phys. Rev.* E **94** 052101
[22] Kato A and Tanimura Y 2016 *J. Chem. Phys.* **145** 224105
[23] Thomas G, Siddharth N, Banerjee S and Ghosh S 2018 *Phys. Rev.* E **97** 062108
[24] Whitney R S 2018 *Phys. Rev.* B **98** 085415
[25] Gemmer J, Michel M and Mahler G 2004 *Quantum Thermodynamics–Emergence of Thermodynamic Behavior Within Composite Quantum Systems* 1st edn (Berlin, Berlin: Springer)
[26] Huber G, Schmidt-Kaler F, Deffner S and Lutz E 2008 *Phys. Rev. Lett.* **101** 070403
[27] Campisi M, Hänggi P and Talkner P 2011 *Rev. Mod. Phys.* **83** 771
[28] Mazzola L, De Chiara G and Paternostro M 2013 *Phys. Rev. Lett.* **110** 230602
[29] Batalhão T B, Souza A M, Mazzola L, Auccaise R, Sarthour R S, Oliveira I S, Goold J, De Chiara G, Paternostro M and Serra R M 2014 *Phys. Rev. Lett.* **113** 140601
[30] An S, Zhang J-N, Um M, Lv D, Lu Y, Zhang J, Yin Z-Q, Quan H T and Kim K 2015 *Nat. Phys.* **11** 193
[31] Sagawa T and Ueda M 2008 *Phys. Rev. Lett.* **100** 080403
[32] Jacobs K 2009 *Phys. Rev.* A **80** 012322
[33] Sagawa T and Ueda M 2010 *Phys. Rev. Lett.* **104** 090602
[34] Deffner S 2013 *Phys. Rev.* E **88** 062128
[35] Funo K, Watanabe Y and Ueda M 2013 *Phys. Rev.* E **88** 052121
[36] Goold J, Huber M, Riera A, del Rio L and Skrzypczyk P 2016 *J. Phys. A: Math. Theor.* **49** 143001
[37] Strasberg P, Schaller G, Brandes T and Esposito M 2017 Quantum and Information Thermodynamics: A Unifying Framework Based on Repeated Interactions *Phys. Rev.* X **7** 021003
[38] Camati P A, Peterson J P S, Batalhão T B, Micadei K, Souza A M, Sarthour R S, Oliveira I S and Serra R M 2016 *Phys. Rev. Lett.* **117** 240502
[39] Ciampini M A, Mancino L, Orieux A, Vigliar C, Mataloni P, Paternostro M and Barbieri M 2017 *npj Quantum Information* **3** 10
[40] Cottet N, Jezouin S, Bretheau L, Campagne-Ibarcq P, Ficheux Q, Anders J, Auffèves A, Azouit R, Rouchon P and Huard B 2017 Observing a quantum Maxwell demon at work *Proceedings of the National Academy of Sciences (PNAS)* **114**

[41] Masuyama Y, Funo K, Murashita Y, Noguchi A, Kono S, Tabuchi Y, Yamazaki R, Ueda M and Nakamura Y 2018 *Nat. Commun.* **9** 1291
[42] Xiong T P, Yan L L, Zhou F, Rehan K, Liang D F, Chen L, Yang W L, Ma Z H, Feng M and Vedral V 2018 *Phys. Rev. Lett.* **120** 010601
[43] Naghiloo M, Alonso J J, Romito A, Lutz E and Murch K W 2018 *Phys. Rev. Lett.* **121** 030604
[44] Boykin P O, Mor T, Roychowdhury V, Vatan F and Vrijen R 2002 Algorithmic cooling and scalable NMR quantum computers *Proceedings of the National Academy of Sciences* **99** 3388
[45] Baugh J, Moussa O, Ryan C A, Nayak A and Laflamme R 2005 *Nature* **438** 470
[46] Liuzzo-Scorpo P, Correa L A, Schmidt R and Adesso G 2016 Thermodynamics of Quantum Feedback Cooling *Entropy* **18** 48
[47] Rodríguez-Briones N A, Martín-Martínez E, Kempf A and Laflamme R 2017 *Phys. Rev. Lett.* **119** 050502
[48] Schmidt R, Maniscalco S and Ala-Nissila T 2016 *Phys. Rev.* A **94** 010101
[49] Elouard C, Herrera-Martí D, Huard B and Auffèves A 2017 *Phys. Rev. Lett.* **118** 260603
[50] Scarani V, Ziman M, Štelmachovič P, Gisin N and Bužek V 2002 *Phys. Rev. Lett.* **88** 097905
[51] Ciccarello F and Giovannetti V 2013 *Phys. Scr.* **T153** 014010
[52] Ciccarello F and Giovannetti V 2017 *Quantum Measurements and Quantum Metrology* **4** 53
[53] Kretschmer S, Luoma K and Strunz W T 2016 *Phys. Rev.* A **94** 012106
[54] Campbell S, Ciccarello F, Palma G M and Vacchini B 2018 *Phys. Rev.* A **98** 012142
[55] Çakmak B, Campbell S, Vacchini B, Müstecaplıoğlu O E and Paternostro M 2019 *Phys. Rev.* A **99** 012319
[56] Jin J, Giovannetti V, Fazio R, Sciarrino F, Mataloni P, Crespi A and Osellame R 2015 *Phys. Rev.* A **91** 012122
[57] Cialdi S, Rossi M A C, Benedetti C, Vacchini B, Tamascelli D, Olivares S and Paris M G A 2017 *Appl. Phys. Lett.* **110** 081107
[58] Haase J F, Vetter P J, Unden T, Smirne A, Rosskopf J, Naydenov B, Stacey A, Jelezko F, Plenio M B and Huelga S F 2018 *Phys. Rev. Lett.* **121** 060401
[59] Wang F *et al* 2018 *Phys. Rev.* B **98** 064306
[60] Peng S, Xu X, Xu K, Huang P, Wang P, Kong X, Rong X, Shi F, Duan C and Du J 2018 *Sci. Bull.* **63** 336
[61] Groen J P, Ristè D, Tornberg L, Cramer J, de Groot P C, Picot T, Johansson G and DiCarlo L 2013 *Phys. Rev. Lett.* **111** 090506
[62] Ziman M, Štelmachovič P, Bužek V, Hillery M, Scarani V and Gisin N 2002 *Phys. Rev.* A **65** 042105
[63] Brun T A 2002 *Am. J. Phys.* **70** 719
[64] Gross J A, Caves C M, Milburn G J and Combes J 2018 *Quantum Science and Technology* **3** 024005
[65] Lu D, Brodutch A, Li J, Li H and Laflamme R 2014 *New J. Phys.* **16** 053015
[66] McCloskey R and Paternostro M 2014 *Phys. Rev.* A **89** 052120
[67] Pezzutto M, Paternostro M and Omar Y 2019 *Quantum Science and Technology* **4** 025002
[68] Seah S, Nimmrichter S and Scarani V 2019 *Phys. Rev.* E **99** 042103
[69] Wittemer M, Clos G, Breuer H-P, Warring U and Schaetz T 2018 *Phys. Rev.* A **97** 020102